PERGAMON

International Journal of Multiphase Flow 28 (2002) 1945–1963

International Journal of Multiphase Flow

www.elsevier.com/locate/ijmulflow

Creeping flow past and within a permeable spheroid

P. Vainshtein [a], M. Shapiro [b,*], C. Gutfinger [a]

[a] *Aerosol Research Laboratory, Faculty of Mechanical Engineering, Technion—Israel Institute of Technology, Haifa 32000, Israel*

[b] *Laboratory of Transport Processes in Porous Materials, Faculty of Mechanical Engineering, Technion—Israel Institute of Technology, Haifa 32000, Israel*

Received 12 February 2002; received in revised form 9 September 2002

Abstract

Flow past and within an isolated permeable spheroid directed along its axis of symmetry is studied. The flow velocity field is solved using the Stokes creeping flow equations governing the fluid motion outside the spheroid, and the Darcy equation within the spheroid. Expressions for the hydrodynamic resistance experienced by oblate and prolate spheroids are derived and analyzed. The limiting cases of permeable circular disks and elongated rods are examined. It is shown that the spheroid's resistance varies significantly with its aspect ratio and permeability, expressed via the Brinkman parameter.

Keywords: Porous particles; Permeability; Creeping flow; Flow resistance; Porous boundary; Prolate–oblate spheroids

1. Introduction

Flows past particles of various shapes, such as rigid spheres, spheroids, and cylinders have been studied quite extensively. A wide variety of analytical and numerical methods had been used to obtain solutions for a broad range of geometric and flow parameters. For excellent compilations of these results, the reader is referred to the monographs by Happel and Brenner (1983) and Clift et al. (1978). These books, however, do not consider the flows past porous particles. Indeed, going through the literature, one finds very little information on this subject as compared to flow past solid bodies. This is in spite of the fact that porous particles are widely used in technology, in particular in chemical process industries. Porous pellets are used extensively in catalytic reactors.

* Corresponding author. Fax: +972-48-294-923.
E-mail address: mersm01@tx.technion.ac.il (M. Shapiro).

0301-9322/02/$ - see front matter
PII: S0301-9322(02)00106-4

It has been shown that convective transport in these particles might enhance effectiveness factors and improve selectivity of chemical reactors (Nir and Pismen, 1977). Porous particles are frequently found in the atmosphere and in other environmental systems, where they are normally formed by vapor condensation–coagulation processes (Pruppacher and Klett, 1978).

Flow inside porous bodies is usually described by the Darcy equation (Adler, 1992). Such a description of the flow is often combined with the Navier–Stokes equations for modeling the flow outside the bodies. To close the problem, one requires that these two flow fields satisfy appropriate boundary conditions formulated at the surface of the porous body. Such conditions constitute a controversial subject, extensively discussed in the literature (see below a discussion on this matter). One principal difficulty in rigorous formulation of these conditions stems from the nature of the Darcy equation, which has no shear stress tensor associated with it. One way to overcome this difficulty is to use the Brinkman equation instead, which is endowed by the viscous stress tensor (Scheidegger, 1960).

Several studies of the flow field within and outside porous spheres are limited mainly to low Reynolds numbers. Joseph and Tao (1964) and Sutherland and Tan (1970) calculated the flow field, described by Darcy's law, near and within a permeable sphere. Joseph and Tao (1964) used the no-slip condition for the fluid at the surface of the sphere, with the result that the tangential velocity component is generally not continuous at the surface. On the other hand, Sutherland and Tan (1970) assumed continuity of the tangential velocity component at the sphere surface. Ooms et al. (1970) replaced the Darcy equation by the Brinkman equation for the internal flow field. Neale et al. (1973) generalized this solution, using a hydrodynamic spherical cell model, to address the problem of flow relative to a swarm of permeable spheres. They also compared the hydrodynamic resistance of porous spheres calculated from theories based on the Darcy and Brinkman equations. For low-porosity spheres, these predicted resistances are so close that they could not be distinguished experimentally. However, the hydrodynamic resistance of high-porosity spheres calculated from the Brinkman equation is significantly lower than that obtained from the Darcy equation. Adler (1981) calculated streamlines in and around spherical porous particle, using the velocity field obtained by Neale et al. (1973). Jones (1973) used the Darcy equation to solve the problem of creeping flow around a porous spherical particle containing a rigid concentric spherical core. Haber and Mauri (1983) solved the similar problem when employing the Brinkman equation. The experimental data of Matsumoto and Suganuma (1977) on settling velocity of steel wool porous spheres was shown to be in excellent agreement with the theoretical predictions of Ooms et al. (1970) for a wide range of the porosities used. On the other hand, calculations of Sutherland and Tan (1970) fitted only the data for spheres with relatively low-porosity. Nandakumar and Masliyah (1982) studied numerically the flow field inside and around an isolated porous sphere in the range of intermediate Reynolds numbers using the Brinkman equation for the internal flow field. The computed hydrodynamic resistances were found to agree with the experiments on settling of porous spheres, machined from semi-rigid plastic foam (Masliyah and Polikar, 1980). In a more recent work Feng and Michaelides (1998) treated this problem using the Darcy law.

In the engineering practice and environment, porous particles often have geometrical shapes, which differ significantly from spherical. The simplest geometry allowing one to study the effect shape of the permeable particles on their settling velocity and drag resistance is spheroidal. We are not aware of any investigations that deal with motion of such particles. The present paper is aimed

to investigate analytically the flow past and within permeable spheroids and determine the hydrodynamic resistance experienced by such particles. We first determine the drag resistance of a permeable oblate spheroidal particle held stationary in a uniform creeping flow. Then the treatment is extended to the comparable prolate spheroidal particle.

2. Problem formulation for an oblate spheroid

Consider creeping flow past and within an oblate permeable spheroid

$$\frac{\rho^2}{a^2}+\frac{z^2}{b^2}=1, \tag{1}$$

where a and b are the spheroid major and the minor semi-axes, respectively, $\rho=\sqrt{x^2+y^2}$ and x, y and z are the Cartesian coordinates. The undisturbed flow velocity U is directed parallel to the axis of revolution of the spheroid (see Fig. 1a), which is held stationary while the fluid streams past and within it.

Outside the spheroid the velocity field is described by the Stokes and continuity equations, respectively,

$$\left.\begin{aligned}&\mu\nabla^2\mathbf{u}=\nabla p\\&\nabla\cdot\mathbf{u}=0\end{aligned}\right\}\quad\text{outside the spheroid,} \tag{2), (3}$$

where μ is the fluid viscosity. The equations for the fluid motion within the porous spheroid of permeability k are the Darcy law and the fluid continuity equation:

$$\left.\begin{aligned}&-\frac{\mu}{k}\widehat{\mathbf{u}}=\nabla\widehat{p}\\&\nabla\cdot\widehat{\mathbf{u}}=0\end{aligned}\right\}\quad\text{inside the spheroid.} \tag{4), (5}$$

Appropriate for the solution of the problem are oblate spheroidal coordinates (ξ,η,φ) (Happel and Brenner, 1983):

$$\rho=c\cosh\xi\sin\eta,\quad z=c\sinh\xi\cos\eta, \tag{6}$$

where

$$c=\sqrt{a^2-b^2},\quad 0\leqslant\xi<\infty,\quad 0\leqslant\eta\leqslant\pi. \tag{7}$$

These coordinates constitute a right-handed orthogonal, curvilinear coordinate system with the following metric coefficients:

$$\begin{aligned}&h=h_1=h_2=1/c(\cosh^2\xi-\sin^2\eta)^{1/2},\\&h_3=1/c\cosh\xi\sin\eta.\end{aligned} \tag{8}$$

The coordinate surfaces $\xi=\text{const}$ constitute a family of confocal oblate spheroidal surfaces defined by Eq. (1) (see Fig. 1a). The focal circle lies in the plane $z=0$ and corresponds to the circle $\rho=c$. The coordinate surfaces $\eta=\text{const}$ define a family of confocal hyperboloids of revolution with $o-z$ being their axis of rotation. $0<\eta<\pi/2$ correspond to the region $z>0$, whereas values of $\pi/2<\eta<\pi$ belong to the region $z<0$. For more details on properties of this coordinate

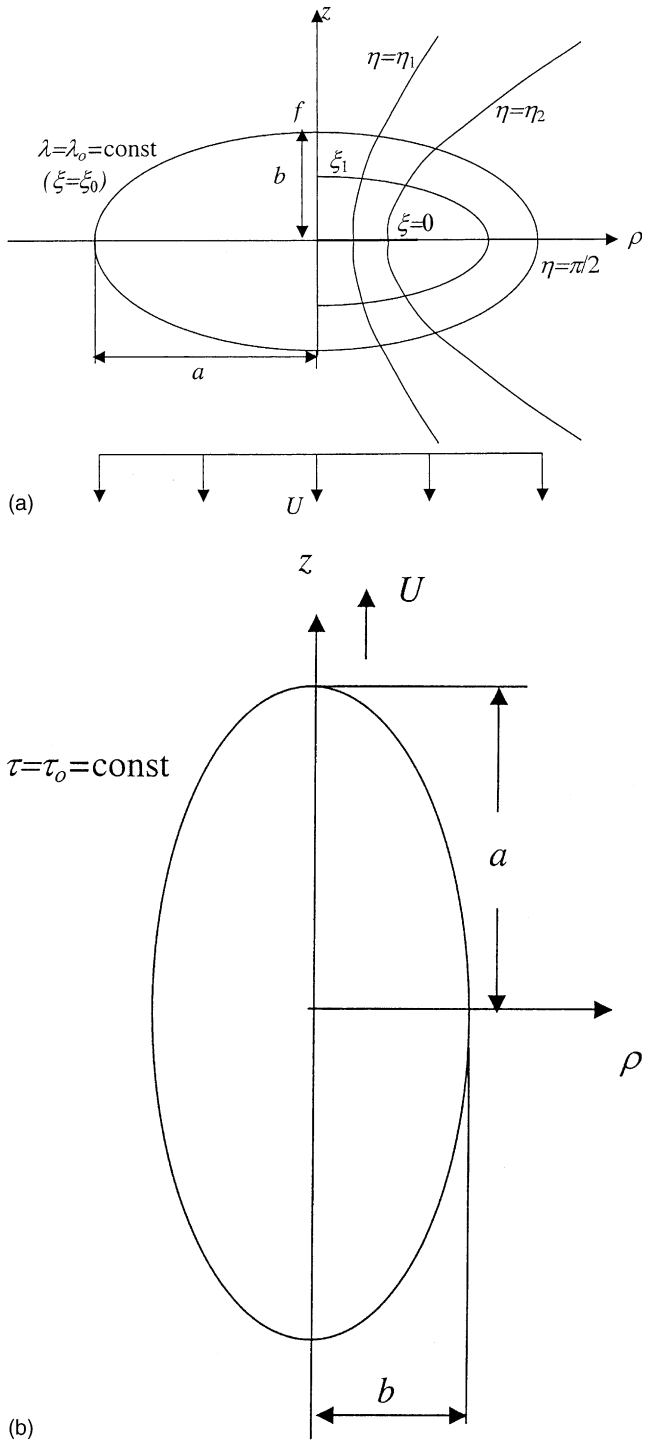

Fig. 1. (a) Oblate spheroid in a uniform flow. Spheroidal coordinate system. (b) Prolate spheroid in a uniform flow.

system, the reader is referred to the book by Happel and Brenner (1983). We designate the particle surface by $\xi = \xi_0$. Then, one has from Eqs. (1), (6) and (7)

$$\xi_0 = \frac{1}{2}\ln\frac{a+b}{a-b}. \tag{9}$$

The limiting case of a sphere is obtained by setting $\xi_0 \to \infty$. Large distances from the origin are equivalent to large values of ξ, i.e. $\xi \to \infty$ as $r = \sqrt{\rho^2 + z^2} \to \infty$. Now, for brevity, we put

$$\lambda = \sinh\xi, \quad \zeta = \cos\eta. \tag{10}$$

With this substitutions we have, from Eq. (6),

$$\rho = c\sqrt{\lambda^2+1}\sqrt{1-\zeta^2}, \quad z = c\lambda\zeta. \tag{11}$$

The variables λ and ζ range over the values $0 \leqslant \lambda < \infty$, $-1 \leqslant \zeta \leqslant 1$. The following relations obtained from Eq. (10) prove useful in the sequel:

$$\frac{\partial}{\partial\xi} = \sqrt{\lambda^2+1}\frac{\partial}{\partial\lambda}, \quad \frac{\partial}{\partial\eta} = -\sqrt{1-\zeta^2}\frac{\partial}{\partial\zeta}. \tag{12}$$

Using Eqs. (9) and (10), one may express λ_0, corresponding to the particle surface, in terms of the basic dimensions of the spheroid, a and b, as

$$\lambda_0 = \frac{b}{c} = \left[\left(\frac{a}{b}\right)^2 - 1\right]^{-1/2}. \tag{13}$$

Eqs. (2), (3) and (4), (5) may now be rewritten in terms of the Stokes stream functions, ψ and $\widehat{\psi}$, as follows (Happel and Brenner, 1983):

$$E^4\psi = 0, \tag{14}$$

$$E^2\widehat{\psi} = 0, \tag{15}$$

where $E^4 = E^2(E^2)$ and the operator E^2 is

$$E^2 = \frac{1}{c^2(\lambda^2+\zeta^2)}\left[(\lambda^2+1)\frac{\partial^2}{\partial\lambda^2} + (1-\zeta^2)\frac{\partial^2}{\partial\zeta^2}\right]. \tag{16}$$

Using Eqs. (2), (6), (10) and (12), one may establish the relations between the pressure and the stream function for the external flow, as follows:

$$\begin{aligned}\sqrt{\lambda^2+1}\frac{\partial p}{\partial\lambda} &= \frac{\mu}{\rho}\sqrt{1-\zeta^2}\frac{\partial}{\partial\zeta}(E^2\psi),\\ \sqrt{1-\zeta^2}\frac{\partial p}{\partial\zeta} &= -\frac{\mu}{\rho}\sqrt{\lambda^2+1}\frac{\partial}{\partial\lambda}(E^2\psi).\end{aligned} \tag{17}$$

Using Eqs. (6), (10) and (15), one rewrites Eq. (4) for the internal flow in the following form:

$$\sqrt{\lambda^2+1}\frac{\partial \widehat{p}}{\partial \lambda} = -\frac{\mu}{k\rho}\sqrt{1-\zeta^2}\frac{\partial \widehat{\psi}}{\partial \zeta},$$
$$\sqrt{1-\zeta^2}\frac{\partial \widehat{p}}{\partial \zeta} = \frac{\mu}{k\rho}\sqrt{\lambda^2+1}\frac{\partial \widehat{\psi}}{\partial \lambda}. \tag{18}$$

The boundary conditions for the stream functions are formulated as follows: Far from the spheroid, the flow is uniform in the negative z-direction. According to Eq. (11), the boundary condition at infinity is

$$\psi \to \frac{1}{2}Uc^2(\lambda^2+1)(1-\zeta^2) \quad \text{as } \lambda \to \infty. \tag{19}$$

We look for a solution, which describes the limiting case of flow past and within a porous sphere, where the stream function is finite as $r \to 0$. Therefore, the solution in the interior is required to reproduce the known solution of Joseph and Tao (1964) and Sutherland and Tan (1970):

$$\widehat{\psi}(\lambda,\zeta) \to \widehat{\psi}_s(r,\zeta) = \frac{3Uk}{4a^2+6k}\rho^2 \quad \text{as } \lambda_0 \to \infty. \tag{20}$$

The normal velocity component is required to be continuous at the boundary of the spheroid

$$\left.\frac{\partial \psi(\lambda,\zeta)}{\partial \zeta}\right|_{\lambda_0} = \left.\frac{\partial \widehat{\psi}(\lambda,\zeta)}{\partial \zeta}\right|_{\lambda_0}. \tag{21}$$

It follows from this condition that the stream function is continuous at the boundary. The tangential velocity component has also this property (Sutherland and Tan, 1970)

$$\left.\frac{\partial \psi(\lambda,\zeta)}{\partial \lambda}\right|_{\lambda_0} = \left.\frac{\partial \widehat{\psi}(\lambda,\zeta)}{\partial \lambda}\right|_{\lambda_0}. \tag{22}$$

One more condition is required to complete the formulation of the problem. Note that no restriction can be imposed at the boundary on the shear stress because the Darcy flow does not possess this quantity. However, there always exists a point f at the boundary of any permeable body where the tangential velocity component vanishes. For our spheroidal particle, this point is the frontal symmetry point f (see Fig. 1a). Along the streamline, going through the frontal point, the flow may be considered potential. The situation is quite similar to that occurring in flows past impermeable bodies in the vicinity of a stagnation point. Hence, the pressure has to be continuous at the frontal point, since flow inertia is neglected in Eqs. (2) and (4). Therefore, we use this feature as our last boundary condition,

$$p(\lambda,1)|_{\lambda_0} = \widehat{p}(\lambda,1)|_{\lambda_0}. \tag{23}$$

2.1. Discussion of the model

When a viscous fluid flows over the surface of a porous body, the effects of viscous shear can penetrate into the porous medium to form a boundary layer region adjacent to the interface (Beavers and Joseph, 1967). The Darcy law—Eq. (4), is not generally compatible with the exis-

tence of such a region, because no stress term is associated with this equation. The Darcy equation is considered appropriate only for low-porosity systems, wherein the thickness of the internal boundary layer is negligible. For highly porous materials the effect of the boundary layer may be significant. Because of this, the boundary condition of Eq. (22) is used in conjunction with Darcy's law only for low-porosity systems (Sutherland and Tan, 1970).

An alternative approach is to employ Brinkman's extension of the Darcy equation (which includes the viscous stress), as did Ooms et al. (1970) and Neale et al. (1973) to examine the flow through a porous sphere. In this case, the boundary condition of Eq. (22) is obviously applicable to materials of any porosity. An additional boundary condition, namely, the shear stress continuity at the boundary of the sphere, is also invoked to complete the formulation of the problem (19)–(23).

The particle porosity affects its hydrodynamic resistance. This is described in terms of the following dimensionless parameters:

$$\Omega = \frac{F_z}{F_{\mathrm{zim}}} \tag{24}$$

which is the ratio of resistances experienced by permeable and impermeable particles of the same shape, and the Brinkman parameter

$$\beta = \frac{l}{\sqrt{k}}, \tag{25}$$

where l is a characteristic particle dimension. For a sphere, l is equal to its radius. For a spheroid, it is equal to its equatorial radius, such that for an oblate spheroid (1) $l = a$ and for a prolate spheroid (see below Section 4) $l = b$. This parameter characterizes the relative effect of particle permeability on Ω.

Neale et al. (1973) compared the resistances experienced by a permeable sphere calculated by the use of the Brinkman equation and from the Darcy equation, both employed together with boundary condition of Eq. (22). These two models give asymptotically identical results when $\beta \to \infty$. For permeable spheres characterized by $5 < \beta < 20$, the models predict $0.764 < \Omega < 0.946$ and $0.943 < \Omega < 0.996$, respectively. In particular, the difference between these predictions exceeds 10% for $\beta < 10$. An experimental verification of these predictions has been done by Matsumoto and Suganuma (1977) for porous spheres made from steel wool. It was found that for $10 < \beta < 200$ the experimental values of Ω agree with both theories, namely, the difference between the two theoretical predictions in this interval of β is less than the error of measurements. For $5 < \beta < 10$, calculations based on the Brinkman equation appear preferable. Thus, the discrepancy between these two theories is considerable only for particles with $\beta < 10$.

A modified boundary condition was suggested on the tangential velocity at the interface, to be used in conjunction with Darcy's law, which is the so-called slip boundary condition (Beavers and Joseph, 1967):

$$\left(\frac{\partial u_x}{\partial y} - \frac{\alpha}{k^{1/2}} (u_x - \widehat{u}_x) \right) \Bigg|_{y=0} = 0, \tag{26}$$

where y is the coordinate normal to the flat surface coinciding with the x-axis and separating the fluid in the channel and the porous channel's wall. Here u_x is the external fluid velocity and $\widehat{u}_x$ is

the internal velocity determined from Darcy's law. The quantity α is an empirical dimensionless parameter. For small k this condition approaches asymptotically the no-slip condition, $u_x = 0$, as also does condition of Eq. (22). Saffman (1971) derived from statistical arguments a boundary condition for the average velocity at the interface of the flat boundary. This condition has the form of Eq. (26) wherein, however, $\widehat{u}_x$ is negligible up to the leading order of the parameter $k^{1/2}/y \ll 1$. His derivations use the condition of fluid pressure continuity across the surface, which is valid both for the flat and spherical boundary. Note that expression (26), with $\widehat{u}_x = 0$ and $\alpha = 1$ may be derived from the exact solution of flow past and within the porous sphere based on the Brinkman equation (Neale et al., 1973; Haber and Mauri, 1983). However, Saffman's simplification of Eq. (26) is inapplicable to the boundary of an arbitrary shape, since, as it is demonstrated below, the pressure is not continuous across the boundary of a general shape. The generalization of boundary condition by Beavers and Joseph (1967) implies that $\alpha(u_x - \widehat{u}_x)/k^{1/2}$ is proportional to the shear stress at the surface. It was used in studies concerning the flow past spherical shells (Jones, 1973) and shear flow past porous particles (Nir, 1976). Generally, representation (26) cannot be directly used as a boundary condition, because the parameter α depends on the structure of the porous material and the shape of the body (Beavers and Joseph, 1967; Beavers et al., 1970; Taylor, 1971; Sahraoui and Kaviany, 1992).

The value of parameter α has been experimentally determined for the flow in a channel with a permeable wall (Beavers and Joseph, 1967; Beavers et al., 1970). Beavers and Joseph (1967) conducted experiments with several porous metals and axolites (compact granular materials)—to determine α. Their experiments yielded $\alpha = 0.1$ for two axolites and $\alpha = 0.8$, 1.5 and 4 for three metals. Beavers et al. (1970) performed experiments, using an improved apparatus and instrumentation, with a metal made of metallic fibers (specifically, nickel) to confirm that $\alpha = 0.1$. Taylor (1971) investigated experimentally and theoretically the flow past a model porous medium—a plate with deep rectangular grooves aligned with the flow—and found that α has a minimum of 1.3 and increases several times beyond this value as the walls between the grooves become thinner. Sahraoui and Kaviany (1992) investigated numerically the flow past arrays of circular cylinders and found that for a square array α increases from 1.2 to 4 as the porosity of the array increases. They also showed that α may be as low as 0.4 when cylinders in the outermost row are not aligned. Summarizing, one can state that α may vary by at least a factor of 10, depending on the geometry and the porous material's structure.

In the present study, we use Darcy's law together with the boundary condition of Eq. (22) to obtain a closed-form analytical solution of the problem. Although both the Stokes and the Brinkman equations are separable in the spheroidal coordinate system, employment of the Brinkman model in our simple analytical method leads to much more involved calculations resulting from the higher order of this equation.

Some comments are also in order on the boundary condition given by Eq. (23). Of course, when considering the Brinkman equation, the correct boundary condition to be used in place of (23) at the boundary of a permeable spheroid is continuity of the normal stress, which includes both the hydrostatic pressure and the viscous terms (Haber and Mauri, 1983). Note that continuity of the pressure at the frontal point of the spheroid is, however, an inherent peculiarity of the potential nature of the flow in this region. The solution based on the Darcy equation is unable to describe the flow structure within a porous layer of thickness $O(\beta^{-1})$ adjacent to the interface, where the viscous stresses are significant. Outside this internal layer, the viscous stress is insignificant. As

such, one cannot use the condition of continuity of the normal stresses at the surface of the spheroid. We employ continuity of the pressure only at the frontal point of the spheroid to close the problem mathematically, as will be shown below. This approach is justified for low-porosity particles, i.e., large β.

Since the fluid is considered incompressible, the internal and external pressure distributions along the interface ($\widehat{p}(\lambda_0,\zeta)$, $p(\lambda_0,\zeta)$) are determined by the corresponding velocity distributions. That is why these functions along the particle boundary are generally different. The pressure distribution across the curved surface of the spheroid is generally not continuous. Indeed, the fluid pressure distribution, $p(\lambda_0,\zeta)$, is determined by the vorticity, $E^2\psi$ (Eq. (17)). When the Brinkman equation is used, $\widehat{p}(\lambda_0,\zeta)$ is determined by the vorticity and the volumetric force $\mu\widehat{u}/k$. In our case, the Darcy equation is employed; hence $\widehat{p}(\lambda_0,\zeta)$ is determined by the latter force only (Eq. (18)).

In the particular case of flow past and within a permeable sphere, discussed below, the internal and external pressure distributions with respect to the meridian angle turn out to be identical (see also Joseph and Tao, 1964; Sutherland and Tan, 1970; Ooms et al., 1970; Neale et al., 1973). This identity apparently occurs due to a specific symmetry of the spherical geometry. When the Brinkman equation is used, the normal viscous stress distributions are identical as well. Therefore, the boundary condition of pressure continuity at the sphere surface, used by Ooms et al. (1970) and Neale et al. (1973), turns out to be equivalent to the condition of continuity of the normal stresses. Joseph and Tao (1964), Sutherland and Tan (1970) and Feng and Michaelides (1998) formulated continuity of pressure at the surface of a porous sphere as a boundary condition, when employing the Darcy equation. Due to peculiarity of the spherical geometry mentioned above, this condition is equivalent to pressure continuity at the sphere's frontal point, as mentioned above. However, our condition is less restrictive, since it allows one to employ the Darcy equation when calculating flows past and within porous particles of non-spherical form.

3. Solution of the problem and results

Condition of Eq. (19) suggests a trial solution of Eqs. (14) and (16) in the form

$$\psi = (1-\zeta^2)g(\lambda), \tag{27}$$

where $g(\lambda)$ is a function to be determined. Upon substitution of (27) into Eq. (16), one obtains

$$E^2\psi = \frac{(1-\zeta^2)}{c^2(\lambda^2+\zeta^2)}G(\lambda), \tag{28}$$

where we have set

$$G(\lambda) = (\lambda^2+1)g''(\lambda) - 2g(\lambda). \tag{29}$$

A second application of the operator E^2 to Eq. (28) gives

$$E^4\psi = \frac{(\lambda^2+1)(1-\zeta^2)}{c^2(\lambda^2+\zeta^2)^3}[4(G-\lambda G') + (\lambda^2+\zeta^2)G'']. \tag{30}$$

To satisfy Eq. (14) the term in square brackets of (30) must vanish. However, as G depends only on λ, this can occur only if the relations $G''=0$ and $G-\lambda G'=0$ are simultaneously satisfied: This results in the following solution for the stream function (Happel and Brenner, 1983):

$$\psi = (1-\zeta^2)\left\{ -\frac{1}{2}C_1\lambda + \frac{1}{2}C_2[\lambda - (\lambda^2+1)\operatorname{arccot}\lambda] + C_3(\lambda^2+1)\right\}. \tag{31}$$

The part of the preceding solution involving an arbitrary constant C_1 is a solution of $E^4\psi = 0$. The remainder of the solution involving the constants C_2 and C_3 satisfies $E^2\psi = 0$ (Happel and Brenner, 1983), thereby resulting in $G = 0$ (see Eq. (28)). We seek a solution of Eq. (15) for $\widehat{\psi}$ in the form (27) as well. In view of the above considerations this solution has a form

$$\widehat{\psi} = (1-\zeta^2)\left\{ \frac{1}{2}A_2[\lambda - (\lambda^2+1)\operatorname{arccot}\lambda] + A_3(\lambda^2+1)\right\}, \tag{32}$$

where A_2 and A_3 are arbitrary constants.

Using Eq. (31), one may rewrite Eq. (17) for the pressure in the external region as

$$\begin{aligned} \frac{\partial p}{\partial \lambda} &= -\frac{\mu C_1}{c^3(\lambda^2+1)}\frac{\partial}{\partial \zeta}\left(\frac{(1-\zeta^2)\lambda}{\lambda^2+\zeta^2}\right), \\ \frac{\partial p}{\partial \zeta} &= -\frac{\mu C_1}{c^3}\frac{\partial}{\partial \lambda}\left(\frac{\lambda}{\lambda^2+\zeta^2}\right). \end{aligned} \tag{33}$$

Solution of Eq. (33) is

$$p = \frac{\mu C_1}{c^3}\frac{\zeta}{\lambda^2+\zeta^2} + p_\infty, \tag{34}$$

where p_∞ is the uniform pressure at infinity ($\lambda \to \infty$). Using Eq. (32), one may rewrite the equations, Eq. (18) for the pressure in the internal region as

$$\begin{aligned} \frac{\partial \widehat{p}}{\partial \lambda} &= \frac{2\zeta\mu}{kc}\left\{\frac{1}{2}A_2\left[\frac{\lambda}{\lambda^2+1} - \operatorname{arccot}\lambda\right] + A_3\right\}, \\ \frac{\partial \widehat{p}}{\partial \zeta} &= \frac{\mu}{kc}\{A_2[1-\lambda\operatorname{arccot}\lambda] + 2A_3\lambda\}. \end{aligned} \tag{35}$$

Solution of Eq. (35) is

$$\widehat{p} = \frac{2\mu\zeta}{kc}\left\{\frac{1}{2}A_2[1-\lambda\operatorname{arccot}\lambda] + A_3\lambda\right\} + p_\infty, \tag{36}$$

where due to the anti-symmetry of the pressure distribution about $\zeta = 0$, one sets as p_∞ the constant of integration.

The boundary condition at infinity, Eq. (19), obviously requires that

$$C_3 = \frac{1}{2}Uc^2. \tag{37}$$

Observing Eq. (11), one concludes that condition (20) requires that in Eq. (32)

$$A_2 = 0. \tag{38}$$

Now, in order to satisfy the required set of boundary conditions, stipulated in Eqs. (21)–(23) the other arbitrary constants in (31) and (32) must be

$$C_1 = \frac{2Uc^4}{k}\frac{\lambda_0(\lambda_0^2+1)}{\Delta_a}, \quad C_2 = -\frac{Uc^4}{k}\frac{\lambda_0(\lambda_0^4-1)}{\Delta_a}, \quad A_3 = Uc^2\frac{1}{\Delta_a},$$
$$\Delta_a = \frac{c^2}{k}[\lambda_0 - (\lambda_0^2-1)\operatorname{arccot}\lambda_0]\lambda_0(\lambda_0^2+1) + 2, \tag{39}$$

that yields a solution for the velocity fields, which also satisfies condition (20).

Using Eqs. (34), (36) and (39), one obtains the solutions for the pressure at the boundary of the spheroid corresponding to the external and internal regions, respectively,

$$p - p_\infty = \frac{2\mu cU}{k}\frac{\lambda_0(\lambda_0^2+1)}{\Delta_a}\frac{\zeta}{\lambda_0^2+\zeta^2}, \tag{40}$$

$$\widehat{p} - p_\infty = \frac{2\mu cU}{k}\frac{\lambda_0}{\Delta_a}\zeta. \tag{41}$$

It can be seen that with the exception of the frontal point ($\zeta = 1$), the external pressure is generally higher than the internal one. However, for flow past a sphere, $\lambda_0 \to \infty$, the external and internal interfacial pressure distributions are identical (Sutherland and Tan, 1970).

In the limiting case of flow past a circular disk, i.e., when $\lambda_0 \to 0$ one obtains

$$p - p_\infty = \frac{\mu cU}{k}\frac{\lambda_0}{\zeta}, \tag{42}$$

$$\widehat{p} - p_\infty = \frac{\mu cU}{k}\lambda_0\zeta. \tag{43}$$

The pressure difference is now most significant. Note that the external pressure tends to infinity when one approaches the edge of the disk, $\zeta \to 0$. At the same time, the internal interfacial pressure approaches zero. Therefore, the difference between the external and internal pressures increases as one approaches the edge of the disk.

The solution obtained for the internal pressure (see Eqs. (36), (38) and (39)) is found from the Darcy and continuity equations (see Eqs. (4), (5)). As all solutions of these equations, it obeys the Laplace's equation. The corresponding solution for the stream function (see Eqs. (32), (38) and (39)) satisfies the boundary conditions of Eqs. (21) and (22). Any solution for the pressure field satisfying continuity condition (40) across the interface will apparently lead to a solution for the velocity field violating boundary conditions (21) and (22).

Some streamlines derived from Eqs. (31), (32), (38) and (39) are plotted (in the plane z, ρ) at $b/a = 0.75$ in Figs. 2–4 for $\beta_a = ak^{-1/2} = 1$, 10, 50 (cf Eq. (25)). It is seen that the higher the porosity of the medium the closer are the streamlines to straight lines, and the lower the porosity—the more the streamlines outside the spheroid resemble those of the flow past an impermeable spheroid. Inside the spheroid, the streamlines are always straight lines. This result is clearly seen from Eqs. (20), (32) and (11), according to which

$$\widehat{\psi} = \frac{A_3}{c^2}\rho^2, \tag{44}$$

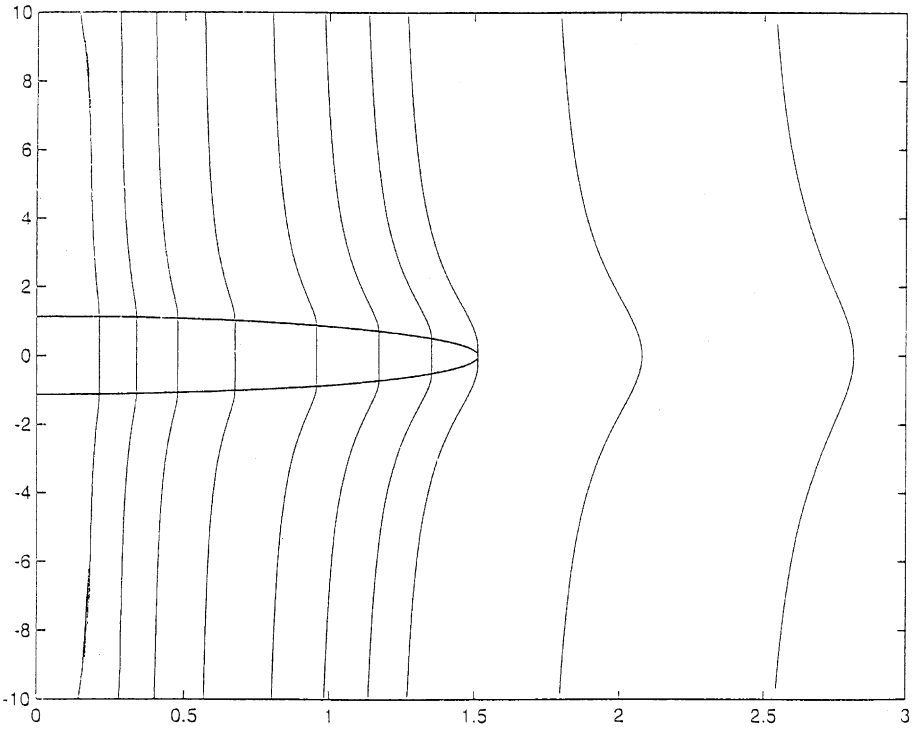

Fig. 2. Streamlines around and within an oblate spheroid for $\beta_a = 1$, $b/a = 0.75$.

where A_3 is defined in Eq. (39). The velocity components are obtained in the form

$$\widehat{u}_\rho = 0, \quad \widehat{u}_z = -\frac{2A_3}{c^2}. \tag{45}$$

Eqs. (45) show that inside the spheroid the fluid moves with a constant velocity directed along the z-axis. Moreover, it follows from Eqs. (21) and (22), (45) that the tangential velocity component vanishes near the frontal point, as per our comment made in Section 2.

The streamlines are straight inside the porous spheroidal or spherical particles only when the Darcy equation is used. On the contrary, when the Brinkman equation is employed these streamlines are curved (Adler, 1981).

In several applications, it is required to find the flow rate passing through the permeable particle. This is determined by the limiting streamline, characterized, say, by $\rho = \rho_0$, which goes over the edge of the spheroid. Observation of behavior of streamlines presented in Figs. 2–4 reveals that ρ_0 varies from a when $\beta = 0$, to zero when $\beta = \infty$, which agrees with similar result obtained by Adler (1981) for flow past and within porous sphere. Fig. 5 shows the dependences of ρ_0^2/a^2 on β_a^2 for different aspect ratios $1 - b/a = 1$, 0.5 and 0.25. The ratio ρ_0^2/a^2 is an important parameter characterizing the efficiency with which a porous particle collects dispersed particles of much smaller size. This is especially important for the evaluation of aerosol scavenging rates by falling snowflakes (Pruppacher and Klett, 1978). It is seen that the collision efficiency, as characterized by ρ_0^2/a^2 grows as the aspect ratio diminishes.

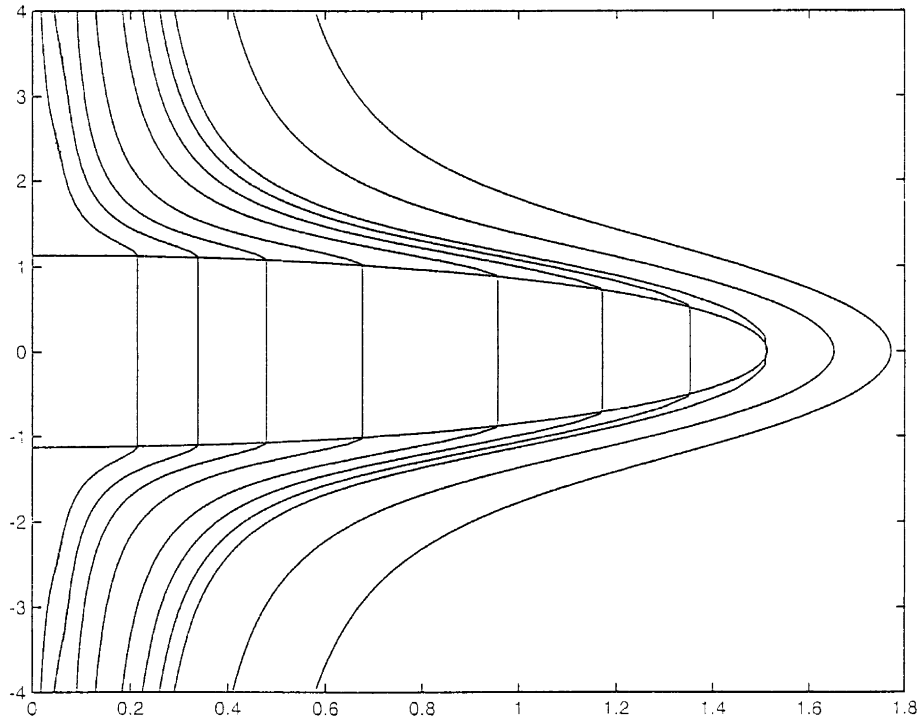

Fig. 3. Streamlines around and within an oblate spheroid for $\beta_a = 10$, $b/a = 0.75$.

Using Eq. (37), one may rewrite Eq. (31) as

$$\psi = \frac{1}{2} U \rho^2 \left\{ 1 - \frac{C_2}{Uc^2} \operatorname{arccot} \lambda - \frac{C_1 - C_2}{Uc^2} \frac{\lambda}{\lambda^2 + 1} \right\}, \tag{46}$$

where C_1 and C_2 are defined in Eq. (39). The corresponding expression for the stream function of an oblate spheroid translating with a velocity U in the positive z-direction may be obtained by subtracting $\rho U^2/2$ from Eq. (46)

$$\tilde{\psi} = -\frac{1}{2} U \rho^2 \left\{ \frac{C_2}{Uc^2} \operatorname{arccot} \lambda + \frac{C_1 - C_2}{Uc^2} \frac{\lambda}{\lambda^2 + 1} \right\}. \tag{47}$$

The force exerted by the fluid on the spheroid can be obtained from the following equation (Payne and Pell, 1960; Happel and Brenner, 1983):

$$F_z = 8\pi\mu c \lim_{\lambda \to \infty} \frac{\lambda \tilde{\psi}}{\rho^2}. \tag{48}$$

Calculating this limit, substituting C_1 from Eq. (39), c from Eq. (7) and using Eq. (13), one obtains the particle's hydrodynamic resistance

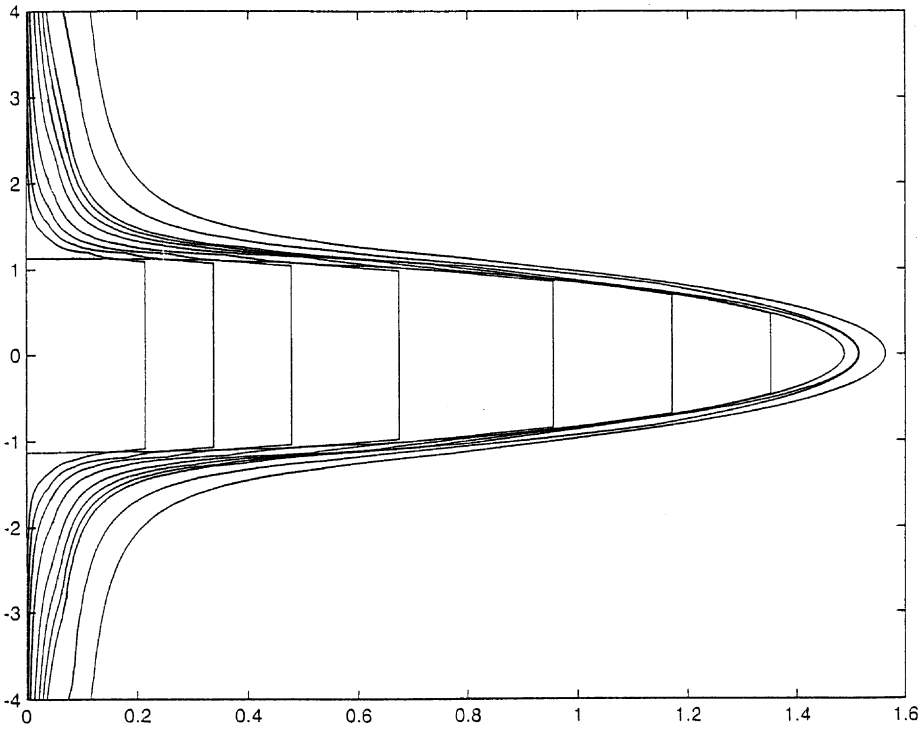

Fig. 4. Streamlines around and within an oblate spheroid for $\beta_a = 50$, $b/a = 0.75$.

$$F_z = -8\pi\mu a U \frac{\beta_a^2}{\beta_a^2[\lambda_0 - (\lambda_0^2 - 1)\operatorname{arccot}\lambda_0]\sqrt{\lambda_0^2 + 1} + 2\sqrt{(\lambda_0^2 + 1)/\lambda_0^2}}. \tag{49}$$

As $\beta_a \to \infty$ this formula reproduces the resistance of an impermeable spheroid F_{zi} (see Happel and Brenner, 1983). Note that the resistance of the oblate spheroid, F_{zi}, is smaller than that of a sphere of radius a, $F_s = -6\pi\mu a U$. Fig. 6 shows the dependence of F_z/F_s on $\bar{\beta}^2 = ab/k$ for different particle aspect ratios. It is seen that the resistance increases when the aspect ratio increases. The ratio F_z/F_s tends to F_{zi}/F_s as $\bar{\beta} \to \infty$.

In the case of flow past a sphere, $\lambda_0 \to \infty$, one obtains from Eq. (49) the resistance of a permeable sphere calculated by Sutherland and Tan (1970). For porous spheres when $10 < \beta_a < 20$ their result predicts $0.984 < \Omega < 0.996$. Hence, it would appear difficult to distinguish between the resistances of permeable and impermeable ($\Omega = 1$) spheres, when β_a is within the above interval. This led Sutherland and Tan (1970) to conclude that an insignificant quantity of fluid will actually permeate through an isolated particle and it can be treated as an impermeable body. This assertion would be correct if the particle could be considered a sphere. However, the geometry of porous particles is often not spherical. Therefore, it is of interest to evaluate Ω from the obtained results for permeable spheroids. At $b/a = 0.25$ and the same interval of β_a, Eq. (49) predicts $0.851 < \Omega < 0.987$. Thus, the effect of permeability on the resistance of oblate spheroids is more pronounced than that for spheres.

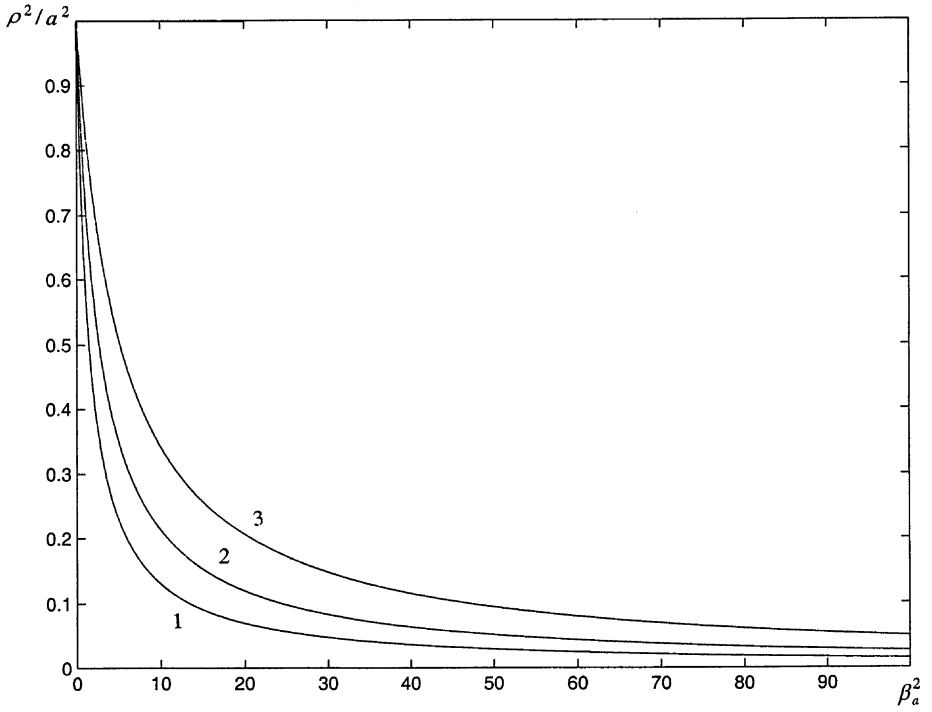

Fig. 5. Flow past and within an oblate spheroid. Dependences of the relative flow rate through the permeable spheroid on β_a^2, for different aspect ratios: $1 - b/a = 1$, $2 - b/a = 0.5$, $3 - b/a = 0.25$.

3.1. Circular disk

Further, for $\lambda_0 = b/a \ll 1$ one obtains an expression for the resistance of a permeable disk, from Eq. (49)

$$F_z = -16\pi\mu a U \frac{\beta_a^2 b/a}{\pi\beta_a^2 b/a + 1}. \tag{50}$$

Substituting the expression for $\beta_a = ak^{-1/2}$ into Eq. (50), one obtains

$$F_z = -16\pi\mu a U \frac{ab}{\pi ab + k}. \tag{51}$$

It is seen from Eq. (51) that the resistance is determined by the parameter $\bar{\beta} = \sqrt{ab/k}$, which is the Brinkman parameter based on the length $\sqrt{ab}$. It is small for high-porosity disks (small $\bar{\beta}$). For low-porosity disks (large $\bar{\beta}$), one should order the limiting procedure to analyze Eqs. (50) and (51). Ordering the limits such that $k \ll ab \ll a^2$, one obtains from Eq. (49) the known expression for the resistance of an impermeable disk, $F_z = -16\mu a U$ (see Happel and Brenner, 1983). If the limiting procedure is ordered such that $ab \ll k \ll a^2$, then, the resistance of a permeable disk approaches zero at the rate governed by ab/k in spite of large a^2/k.

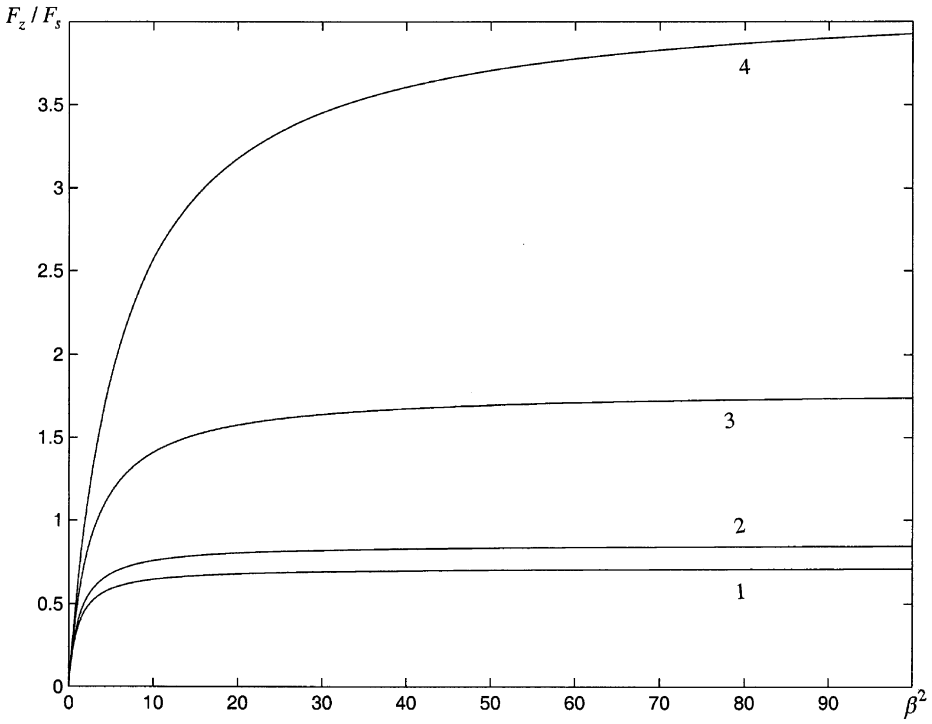

Fig. 6. The dependence of F_z/F_s on $\bar{\beta}^2 = ab/k$ for different aspect ratios. Curves 1, 2 are calculated from Eq. (49) and correspond to oblate spheroids: 1—$b/a = 0.1$, 2—$b/a = 0.5$; Curves 3, 4 are calculated from Eq. (57) and correspond to prolate spheroids: 3—$a/b = 5$, 4—$a/b = 20$.

4. Motion of a permeable prolate spheroid

The motion of a porous prolate spheroid parallel to its axis of revolution (Fig. 1b) is calculated in a manner similar to that employed in the previous sections. The coordinates appropriate to this problem are prolate spheroidal coordinates, (ξ, η, φ), which are similar to those given by Eqs. (6) and (7)

$$\rho = c \sinh \xi \sin \eta, \quad z = c \cosh \xi \cos \eta. \tag{52}$$

For conciseness, we further set

$$\tau = \cosh \xi, \quad \zeta = \cos \eta, \tag{53}$$

so that the surfaces $\tau = \text{const}$ are prolate spheroids. We designate the particular spheroids of interest by τ_0. It is shown by Happel and Brenner (1983) that by substituting $\lambda = i\tau$ and $c = -ic$ in the relations already obtained for an oblate spheroid, λ_0, one obtains the solution of the analogous problem for the prolate spheroid, τ_0. Note that in Fig. 1b the polar and equatorial radii are a and b, respectively, so that the meanings of a and b are interchanged. In both cases a is the longest of the two semi-axes.

Thus, the solutions for the pressure at the boundary of the prolate spheroid corresponding to the external and internal regions as obtained from Eqs. (40) and (41) as

$$p - p_\infty = \frac{2\mu c U}{k} \frac{\tau_0(\tau_0^2 - 1)}{\Delta_b} \frac{\zeta}{\tau_0^2 - \zeta^2}, \tag{54}$$

$$\widehat{p} - p_\infty = \frac{2\mu c U}{k} \frac{\tau_0}{\Delta_b} \zeta, \tag{55}$$

respectively. Here c is defined in Eq. (7) and

$$\Delta_b = \frac{c^2}{k}[(\tau_0^2 + 1)\mathrm{arccoth}\,\tau_0 - \tau_0]\tau_0(\tau_0^2 - 1) + 2. \tag{56}$$

It is seen that with exception of the frontal point ($\zeta = 1$), the external pressure is now smaller than the internal one. Recall that for flow past a sphere ($\tau_0 \to \infty$) the external and internal pressure distributions with respect to the meridian angle are identical.

It may be easily shown that Eq. (45) is also fulfilled in the present case, and within the spheroid the fluid moves with constant velocity directed along the z-axis.

The force on the prolate spheroid is obtained from Eq. (49):

$$F_z = -8\pi\mu b U \times \frac{\beta_b^2}{\beta_b^2[(\tau_0^2 + 1)\mathrm{arccoth}\tau_0 - \tau_0]\sqrt{\tau_0^2 - 1} + 2\sqrt{(\tau_0^2 - 1)/\tau_0^2}}, \tag{57}$$

where β_b is defined by Eq. (25) with $l = b$, i.e. $\beta_b = bk^{-1/2}$. As $\beta_b \to \infty$ Eq. (57) gives the resistance of an impermeable prolate spheroid, F_{zi}. The resistance of the prolate spheroid, F_{zi}, is larger that that of a sphere having the same equatorial radius b. Fig. 6 shows the dependence of F_z/F_s on $\bar{\beta}^2$ for different particle aspect ratios. It is seen that also in the case of a prolate spheroid the resistance increases when the aspect ratio increases. The ratio F_z/F_s tends to F_{zi}/F_s as $\bar{\beta} \to \infty$.

Recall that in the case of flow past a sphere ($\tau_0 \to \infty$) Eq. (57) yields the formula for the resistance of a permeable sphere given by Sutherland and Tan (1970). At $b/a = 0.25$ and $5 < \beta_b < 20$ Eq. (57) predicts $0.961 < \Omega < 0.997$. Thus, the effect of permeability on the resistance of prolate spheroids is less than that of spheres where $0.943 < \Omega < 0.996$.

4.1. Elongated rod

When the major axis, a, of the prolate spheroid is much greater than its equatorial radius, b, the spheroid resembles a long thin rod. In this limiting case

$$\tau_0 = \left[1 - \left(\frac{b}{a}\right)^2\right]^{-1/2} \approx 1 + \frac{1}{2}\left(\frac{b}{a}\right)^2, \tag{58}$$

$$\mathrm{arccoth}\,\tau_0 = \frac{1}{2}\ln\frac{\tau_o + 1}{\tau_0 - 1} \approx \ln 2 + \ln\left(\frac{a}{b}\right), \tag{59}$$

$$c \approx a. \tag{60}$$

External and internal pressures are then, from Eqs. (54) and (55),

$$p - p_\infty = \frac{\mu U a}{k} \frac{(b/a)^2}{\beta_b^2\left(\ln 2 + \ln\frac{a}{b} - \frac{1}{2}\right) + 1} \frac{\zeta}{1 - \zeta^2 + (b/a)^2}, \tag{61}$$

$$\widehat{p} - p_\infty = \frac{\mu U a}{k} \frac{1}{\beta_b^2\left(\ln 2 + \ln\frac{a}{b} - \frac{1}{2}\right) + 1} \zeta, \tag{62}$$

respectively. At the frontal point, $\zeta = 1$, the external and internal pressures are equal, according to the boundary condition. They approach zero as $\beta_b \to \infty$. As $\beta_b \to 0$ the pressures approach the following limiting value:

$$p - p_\infty = \widehat{p} - p_\infty = \frac{\mu U a}{k}. \tag{63}$$

It may take place not only at large permeability but also for very thin rods (small b). As $\zeta \to 0$ Eqs. (61) and (62) yield

$$\frac{p - p_\infty}{\widehat{p} - p_\infty} = \left(\frac{b}{a}\right)^2. \tag{64}$$

This means that the external pressure is much smaller than the internal one. The pressures tend to zero in both cases $\beta_b \to \infty$ and $\beta_b \to 0$.

The force on the rod is, from Eq. (57),

$$F_z = -4\pi\mu U a \frac{\beta_b^2}{\beta_b^2\left(\ln 2 + \ln\frac{a}{b} - \frac{1}{2}\right) + 1}. \tag{65}$$

Because of the presence of the logarithmic term, the resistance changes slowly with the ratio a/b. For large values of Brinkman's parameter, $\beta_b \to \infty$, one obtains from Eq. (65) the known formula for an impermeable rod (see Happel and Brenner, 1983). At $b/a = 0.05$ and $5 < \beta_b < 20$ Eq. (65) predicts $0.987 < \Omega < 0.999$. Thus, an elongated rod for such β_b can be treated as an impermeable rod. At $\beta_b \to 0$ Eq. (65) yields

$$F_z = -4\pi\mu U a \frac{b^2}{k}. \tag{66}$$

Hence, the resistance of a permeable rod becomes small as $\beta_b^2 = b^2/k$ diminishes. Note that this can take place not only at high permeability, k, of a medium but also for very thin rods (small b).

5. Conclusions

The creeping flow past and within isolated permeable spheroids has been calculated and discussed. By assuming that Darcy's law governs fluid motion within the particle, a simple and consistent analytical solution is obtained. It has been demonstrated that the hydrodynamic resistance experienced by a spheroid depends significantly on its permeability and aspect ratio. The resistance experienced by an oblate spheroid is smaller than that of a sphere of the same equatorial radius. However, the resistance experienced by a prolate spheroid is larger than that of the

corresponding sphere. The effect of permeability on the resistance of an oblate spheroid is more pronounced than that of a sphere. This property affects the resistance of a prolate spheroid to a lesser extent than in case of a sphere. These peculiarities are most clearly seen in the limiting cases of a permeable circular disk and an elongated rod. The resistance of a low-porosity, but thin enough disk may approach zero, whereas a high-porosity, but long enough rod may be treated as impermeable. Thus, the results obtained indicate that the effects of internal flow permeation depend greatly on particle shape and dimensions. The developed formulae are applicable in practical situations involving in particular aerosol precipitation by falling porous agglomerates.

Acknowledgements

This work was supported by the Fund for the Promotion of Research at Technion—Israel Institute of Technology.

References

Adler, P.M., 1981. Streamlines in and around porous particles. J. Coll. Interface Sci. 81, 531–535.
Adler, P.M., 1992. Porous Media: Geometry and Transports. Butterworth-Heinemann, Stoneham, MA.
Beavers, G.S., Joseph, D.D., 1967. Boundary conditions at a naturally permeable wall. J. Fluid Mech. 30, 197–207.
Beavers, G.S., Sparrow, E.M., Magnuson, R.A., 1970. Experiments on coupled parallel flows in a channel and a bounding porous medium. J. Basic Eng. 92, 843–848.
Clift, R., Grace, J.R., Weber, M.E., 1978. Bubbles, Drops and Particles. Academic Press, New York.
Feng, Z-G., Michaelides, E., 1998. Motion of a permeable sphere at finite but small Reynolds numbers. Phys. Fluids 10, 1375–1383.
Haber, S., Mauri, R., 1983. Boundary conditions for Darcy's flow through porous media. Int. J. Multiphase Flow 9, 561–574.
Happel, J., Brenner, H., 1983. Low Reynolds Number Hydrodynamics. Martinus Nijhoff Publishers, The Hague.
Jones, I.P., 1973. Low Reynolds number flow past a porous spherical shell. Proc. Cambridge Phil. Soc. 73, 231–238.
Joseph, D.D., Tao, L.N., 1964. The effect of permeability on the slow motion of a porous sphere in a viscous liquid. Z. Angew. Math. Mech. 44, 361–364.
Masliyah, J.H., Polikar, M., 1980. Terminal velocity of porous spheres. Can. J. Chem. Eng. 58, 299–302.
Matsumoto, K., Suganuma, A., 1977. Settling velocity of a permeable model flock. Chem. Eng. Sci. 32, 445–447.
Nandakumar, K., Masliyah, J.H., 1982. Laminar flow past a permeable sphere. Can. J. Chem. Eng. 60, 202–211.
Neale, G., Epstein, N., Nader, W., 1973. Creeping flow relative to permeable spheres. Chem. Eng. Sci. 28, 1865–1874.
Nir, A., 1976. Linear shear flow past a porous particle. Appl. Sci. Res. 32, 313–325.
Nir, A., Pismen, L.M., 1977. Simulations of interparticle forced convection, diffusion and reaction in porous catalyst. Chem. Eng. Sci. 32, 35–41.
Ooms, G., Mijnlieff, P.F., Beckers, H.L., 1970. Frictional force exerted by a flowing fluid on a permeable particle, with particular reference to polymer coils. J. Chem. Phys. 53, 4123–4130.
Payne, L.E., Pell, W.H., 1960. The Stokes flow problem for a class of axially symmetric bodies. J. Fluid Mech. 7, 529–549.
Pruppacher, H.R., Klett, J.D., 1978. Microphysics of Clouds and Precipitation. D. Reidel, Dordrecht.
Saffman, P.G., 1971. On the boundary condition at the surface of a porous medium. Stud. Appl. Math. 50, 93–101.
Sahraoui, M., Kaviany, M., 1992. Slip and no-slip velocity boundary condition at the interface of porous, plain media. Int. J. Heat Mass Transfer 35, 927–943.
Scheidegger, A., 1960. The Physics of Flow through Porous Media. University of Toronto Press, Toronto.
Sutherland, D.N., Tan, C.T., 1970. Sedimentation of a porous sphere. Chem. Eng. Sci. 25, 1948–1950.
Taylor, G.I., 1971. A model for the boundary condition of a porous material. Part 1. J. Fluid Mech. 49, 319–326.